ARTICLE

(Carboxymethyl)chitosan-Modified Superparamagnetic Iron Oxide Nanoparticles for Magnetic Resonance Imaging of Stem Cells

Zhilong Shi,[†] K. G. Neoh,[*,†] E. T. Kang,[†] Borys Shuter,[‡] Shih-Chang Wang,[‡] Chyekhoon Poh,[§] and W. Wang[§]

Departments of Chemical and Biomolecular Engineering, of Diagnostic Radiology, and of Orthopaedic Surgery, National University of Singapore, Kent Ridge, Singapore 119260, Singapore

ABSTRACT Magnetic resonance imaging (MRI) is emerging as a powerful tool for in vivo noninvasive tracking of magnetically labeled stem cells. In this work, we present an efficient cell-labeling approach using (carboxymethyl)chitosan-modified superparamagnetic iron oxide nanoparticles (CMCS-SPIONs) as contrast agent in MRI. The CMCS-SPIONs were prepared by conjugating (carboxymethyl)chitosan to (3-aminopropyl)trimethoxysilane-treated SPIONs. These nanoparticles were internalized into human mesenchymal stem cells (hMSCs) via endocytosis as confirmed by Prussian Blue staining and electron microscopy investigation and quantified by inductively coupled plasma mass spectrometry. A MTT assay of the labeled cells showed that CMCS-SPIONs did not possess significant cytotoxicity. In addition, the osteogenic and adipogenic differentiations of the hMSCs were not influenced by the labeling process. The in vitro detection threshold of cells after incubation with 0.05 mg/mL of CMCS-SPIONs for 24 h was estimated to be about 40 cells. The results from this study indicate that the biocompatible CMCS-SPIONs show promise for use with MRI in visualizing hMSCs.

KEYWORDS: superparamagnetic iron oxide nanoparticles • mesenchymal stem cell • (carboxymethyl)chitosan • magnetic resonance imaging

INTRODUCTION

Mesenchymal stem cells (MSCs) have shown great potential in tissue engineering applications because of their ease of isolation and expansion from adult bone marrow aspirates and their versatility for pluripotent differentiation into mesenchymal tissues such as bone, cartilage, fat, muscle, marrow stroma, tendon, and ligament (1, 2). It has been shown recently that human MSCs (hMSCs) can home in to the brain after systemic administration, with subsequent differentiation into neurons (3). After clinical transplantation of stem cells, these donor cells need to be monitored noninvasively and repeatedly in vivo. This challenge cannot be met with traditional immunochemical and histochemical procedures, which require tissue removal at certain time points. Magnetic resonance imaging (MRI) with its excellent spatial resolution has been recognized as one of the best noninvasive imaging modalities in both clinical and research fields. The ability to track specific cell populations via MRI has been extensively studied over the past decade (4−8). Tracking of stem cells by MRI has recently become an emerging application for investigating cell−tissue interactions and guiding the development of effective stem cell therapies (6, 9−14).

To be visualized by MRI, cells need to be magnetically labeled with contrast agents. Among MRI contrast agents, superparamagnetic iron oxide (SPIO) particles have recently received the most attention because of their biocompatibility and strong effects on T_2 and T_2* relaxation (9, 15−17). The incorporation of contrast agents in sufficient quantity into the cells to ensure sensitive and accurate tracking of the labeled cells is an important issue that needs to be addressed. Several methods have been developed to improve SPIO particle internalization. Weissleder and co-workers conjugated the HIV-Tat peptide to dextran-coated iron oxide particles, which greatly enhanced particle uptake into many cell types (18, 19). Bulte and co-workers developed a new contrast agent termed a magnetodendrimer through the suspension of SPIO particles within a dendrimer matrix that efficiently labeled cells for MRI (20). In addition, mixing SPIO particles with common lipofection agents can also promote the internalization process (21, 22).

Commercial contrast agents such as Feridex and Resovist complexed with polycationic transfection agents (TAs) especially poly-L-lysine (PLL) have been used for stem cell labeling (10, 13, 21, 23). The majority of these polycationic TAs are not approved for clinical use by the Food and Drug Administration, and TAs such as PLL are toxic to cells when used by itself. It has been reported that PLL has a relatively narrow tolerated concentration of 10 μg/mL or less in media before causing significant cell death (24). Herein, we present

* To whom correspondence should be addressed. Tel: +65 65162176. Fax: +65 67791936. E-mail: chenkg@nus.edu.sg.
Received for review September 15, 2008 and accepted November 7, 2008
† Department of Chemical and Biomolecular Engineering.
‡ Department of Diagnostic Radiology.
§ Department of Orthopaedic Surgery.
DOI: 10.1021/am8000538

Published on Web 12/10/2008

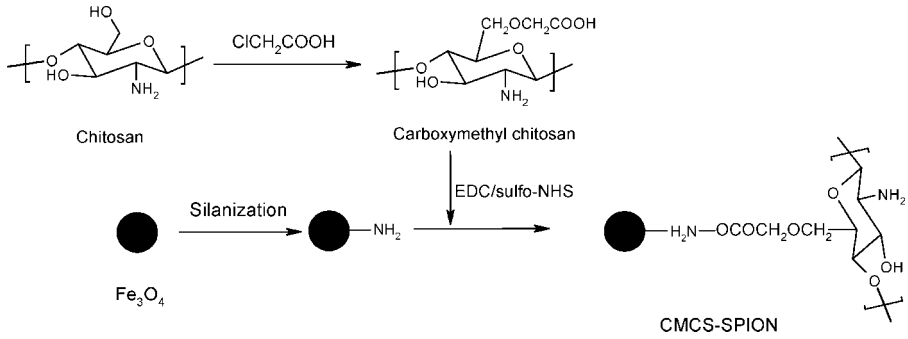

FIGURE 1. Schematic illustration of the immobilization of CMCS on the surface of SPIONs.

a new strategy of using SPIO nanoparticles (SPIONs) coated with biocomparticle carboxymethylated chitosan (CMCS) as contrast agent for labeling hMSCs. Chitosan [poly(1,4-β-D-glucopyranosamine)], an abundant natural biopolymer, is derived by the deacetylation of chitin obtained from the shells of crustaceans. It has great potential as a biomaterial because of its biological activities and low toxicity toward mammalian cells (25). It is expected that a biocompatible polymer coating can prevent agglomeration of the nanoparticles and increase the nonspecific intracellular uptake (26). The carboxymethylation of chitosan increases its solubility in water, and hence the CMCS-coated SPIONs will disperse better in aqueous media. Furthermore, CMCS has been shown to enhance interactions with the cell membrane (27), which may facilitate the uptake of the CMCS-coated SPIONs by the stem cells. In the present work, the uptake of the pristine SPIONs and CMCS-SPIONs into hMSCs was investigated qualitatively and quantitatively. Viability, osteogenic and adipogenic differentiation of the labeled hMSCs were evaluated, and the in vitro detection threshold of the labeled cells was measured with MRI.

MATERIALS AND METHODS

Materials. Ferric chloride hexahydrate ($FeCl_3 \cdot 6H_2O$, >99%), ferrous chloride tetrahydrate ($FeCl_2 \cdot 4H_2O$, >99%), and (3-aminopropyl)trimethoxysilane (APTMS) were obtained from Sigma-Aldrich. Chitosan (CS) was purchased from CarboMer Inc. and refined twice by dissolving it in a dilute acetic acid (HOAc) solution. The solution was filtered, and CS was precipitated with aqueous sodium hydroxide and then dried in a vacuum oven for 24 h at 40 °C. The viscosity-average molecular weight was about 2.2×10^5, as determined by the viscometric method (28). The degree of deacetylation was 84%, as determined by elemental analysis using a Perkin-Elmer model 2400 elemental analyzer (28). All other chemicals were purchased from Sigma-Aldrich unless otherwise stated. Ultrapure water (>18.2 MΩ cm, Millipore Milli-Q system) was used for all experiments and was deoxygenated (by bubbling with N_2 gas) for use in synthesis and surface modification procedures.

Synthesis and Surface Modification of SPIONs. SPIONs (Fe_3O_4) with an average particle size of 6−10 nm were prepared using controlled coprecipitation as reported elsewhere (29). Briefly, 5 mL of an aqueous solution of 1 M $FeCl_3 \cdot 6H_2O$, 0.5 M $FeCl_2 \cdot 4H_2O$, and 0.4 M HCl served as a source of iron. The coprecipitation of magnetite particles was carried out by adding the iron-containing solution to 50 mL of 0.5 M NaOH. The alkaline solution was preheated to 80 °C, and the reaction was carried out for 30 min under N_2 protection to prevent critical oxidation. The particles were collected by sedimentation with the help of an external magnetic field and washed with deoxygenated water and ethanol.

Surface modification of SPION was carried out via silanization to introduce amine groups. In this study, APTMS was anchored to the surface of SPION as described elsewhere (29, 30). For silanization, 100 mg of SPIONs was washed once with methanol (20 mL), thereafter with a mixture of methanol and toluene (20 mL; 1:1, v/v), and finally with toluene alone (20 mL). SPIONs were then dispersed into toluene (20 mL), and 0.5 mL of APTMS [3 mM in a methanol/toluene (1:1, v/v) mixture] was added to the SPION suspension. The suspension was further refluxed at 110 °C for 24 h under a N_2 flow and vigorous stirring. The modified particles were magnetically collected, washed with methanol three times, and dried in a vacuum.

Immobilization of Chitosan on Modified SPIONs. CS was first carboxymethylated to introduce COOH groups for conjugation with the APTMS-modified SPIONs according to the method reported earlier (31, 32). For the carboxymethylation, 10 g of CS and 15 g of sodium hydroxide were added into 100 mL of an isopropyl alcohol/water (80:20, v/v) mixture to swell and alkalize at 60 °C for 1 h. A solution of 15 g of monochloroacetic acid dissolved in 20 mL of isopropyl alcohol was then added dropwise to the reaction mixture over 30 min and reacted for 4 h at the same temperature. The reaction was stopped by the addition of 200 mL of 70% ethanol. The solid was filtered, washed extensively with 70% and 90% ethanol to desalt and dewater, and dried in a vacuum oven at 50 °C. The so-modified chitosan will be denoted as CMCS in the subsequent discussion.

For covalent immobilization of CMCS onto the SPIONs, 50 mg of APTMS-modified SPIONs was added to 10 mL of a 2-(*N*-morpholino)ethanesulfonic acid buffer (MES; 0.1 M, pH = 6.5) containing 25 mg of CMCS, 1-ethyl-3-[3-(dimethylamino)propyl]carbodiimide (EDC; 20 mM), and *N*-hydroxysulfosuccinimide (sulfo-NHS; 50 mM). The mixture was then sonicated for 10 min at 4 °C and shaken for 24 h at room temperature. The CMCS-bound SPIONs were collected under an external magnetic field and washed with a MES buffer and ethanol. The as-prepared SPIONs will be denoted as CMCS-SPIONs in the subsequent discussion. An overall scheme of the functionalization procedure is shown in Figure 1.

Characterization. The chemical composition of the surfaces was analyzed by X-ray photoelectron spectroscopy (XPS) on an AXIS HSi spectrometer (Kratos Analytical Ltd.) with an Al Kα X-ray source (1486.6 eV photons). The details for the XPS measurements are similar to those reported earlier (33). Thermogravimetric analysis (TGA) was carried out with a TGA 2050 thermogravimetric thermal analyzer (TA Instruments, New Castle, DE). The samples (~10 mg) were heated from room temperature to 700 °C at a heating rate of 10 °C/min in air. The size and morphology of the particles were characterized by transmission electron microscopy (TEM; JEOL TEM-2010) at an accelerating voltage of 200 kV. The hydrodynamic diameter of the nanoparticles was obtained from dynamic light scattering measurements performed on a dispersion of the nanoparticles in water (after ultrasonification) using a 90 Plus particle size analyzer (Brookhaven Instruments, Holtsville, NY) at room temperature. Surface charge measurements were performed

with a Zetasizer nanosystem (Malvern Instruments Ltd., Worcestershire, U.K.), and the mean of 10 readings was calculated.

The magnetization measurements were performed at room temperature using a vibrating sample magnetometer (VSM; LakeShore 450-10) with a saturating field of 1 T. The saturation magnetization values were normalized to the mass of nanoparticles to yield the specific magnetization, M_s (emu/g).

Cell Culture and Labeling. hMSCs (Cambrex Bio Science Ltd., Workingham, U.K.) isolated from normal bone marrow donors were cultured in low-glucose Dulbecco's modified Eagle medium (DMEM, GIBCO; Invitrogen, Carlsbad, CA), supplemented with 10% fetal calf bovine serum (FBS; Invitrogen), 100 U/mL penicillin, 100 μg/mL streptomycin, and 1 μg/mL Fungizone. The cells were incubated at 37 °C in a humidified atmosphere of 5% CO_2 and 95% air with the growth medium changed twice every week. The cells were then allowed to grow to about 75% confluence before use. The cultured cells were detached by trypsinization (0.25% trypsin, GIBCO), suspended in a fresh culture medium and used for the designed experiments described below. The cells of passages 2 and 3 were used throughout the study.

Cell labeling was carried out as follows: hMSC (1 mL) suspensions were seeded in a 24-well plate at a density of 2×10^4 cells/well. After 24 h, the medium (1 mL) was aspirated and replaced with either a fresh medium or a medium with the nanoparticles at a concentration of 0.05 mg/mL. The cells were cultured for another 24 h. The cells were then washed with phosphate-buffered silane (PBS; pH = 7.4) extensively to completely remove loosely attached and free particles in the medium before further experiments.

In Vitro Analysis of Nanoparticle Uptake by hMSCs. A Prussian Blue staining assay was used to study the cellular uptake of nanoparticles via optical microscopy. The cells after labeling were washed three times with PBS and subsequently fixed in 4% formaldehyde in PBS for 15 min. For Prussian Blue staining, cells were washed with water, incubated for 30 min with 2% potassium ferrocyanide in 6% HCl, washed with water, and counterstained with Nuclear Fast Red. A Leica DMIL microscope equipped with a Nikon DXM 1200F digital camera was used for imaging.

For TEM viewing, the cells were initially fixed in a Karnovsky's fixative [containing 2% glutaraldehyde and 2.5% paraformaldehyde in a cacodylate buffer (0.1 M, pH 7.4)] for 2 h at room temperature. After two cycles of washing, the cells were postfixed with 1% osmium tetroxide in a cacodylate buffer and dehydrated in a series of increasing concentrations of ethanol. The cells were then incubated with propylene oxide for 30 min and a 1:1 propylene oxide and Spurr's low-viscosity resin mixture overnight at room temperature, embedded in pure resin, and polymerized at 80 °C overnight. Ultrathin sections of about 70 nm were cut using a Reichert-Jung Ultracut E microtome (Leica Microsystems), collected on formvar-coated copper grids, stained with uranyl acetate and lead citrate, and examined with a JEOL 2010F transmission electron microscope.

For quantification of the intracellular uptake of the nanoparticles, the seeding of hMSCs and the incubation with the nanoparticles were carried out as described above. Cells seeded at the same cell density and grown in a 1 mL medium without the nanoparticles constituted the control experiment. After various periods of incubation (2, 6, and 24 h), the cells were washed extensively with PBS to remove loosely attached and free particles in the medium, detached, resuspended, counted, and centrifuged down. The cell pellet was then dissolved in a 37% HCl solution at 40 °C for 30 min. The intracellular iron concentration was quantified using inductively coupled plasma mass spectroscopy (ICP-MS; Perkin-Elmer Elan 6100). Three replicates were measured, and the results were averaged.

Cytotoxicity of Nanoparticles. The cytotoxicity of SPIONs and CMCS-SPIONs was evaluated by determining the viability of hMSCs after incubation with the medium containing the respective nanoparticles. Cell viability testing was carried out via reduction of the MTT reagent (3-[4,5-dimethylthiazol-2-yl]-2,5-diphenyltetrazolium bromide). The MTT assay was performed following the standard procedure with minor modifications (34). Control experiments were carried out using only the complete growth culture medium (serving as the nontoxic control) and 1% Triton X-100 (Sigma) (as the toxic control). hMSC (1 mL) suspensions at a density of 2×10^4 cells/well were seeded in a 24-well plate. After 24 h, the medium was replaced with one containing the nanoparticles at 0.05 mg/mL. The cells were incubated at 37 °C and 5% CO_2 for 6 and 24 h. The culture medium from each well was then removed, and 360 μL of a medium and 40 μL of a MTT solution (5 mg/mL in PBS, 0.1 M, pH = 7.4) were added to each well. After 4 h of incubation at 37 °C and 5% CO_2, the medium was removed and the formazan crystals were solubilized with 400 μL of dimethyl sulfoxide (DMSO; Sigma, Milwaukee, WI) for 15 min. The optical absorbance was then measured at 540 nm (reference wavelength at 630 nm) on a BioTek Powerwave XS microplate reader. The results were expressed as percentages relative to the results obtained with the nontoxic control.

Differentiation of hMSCs. To determine whether the nanoparticles affected the differentiation potential of hMSCs, osteogenic and adipogenic differentiation experiments were conducted. hMSCs were seeded as described above.

For osteogenic differentiation assays, the cells were further cultured in a α-Minimal Essential Medium (α-MEM; GIBCO) supplemented with 10% FBS, 50 μg/mL ascorbic acid, 10 mM sodium β-glycerophosphate, 10 nM dexamethasone, 100 U/mL penicillin, 100 μg/mL streptomycin, and 1 μg/mL Fungizone for 14 days. The alkaline phosphatase activity was determined as previously described (35). The cell layers were washed with PBS and scraped from the surfaces. A cell lysis buffer was added and after sonication and centrifugation, and aliquots of lysate were collected for the analysis of the ALP activity and the total protein level. The ALP activity was determined with respect to the release of *p*-nitrophenol from a *p*-nitrophenyl phosphate substrate. The *p*-nitrophenyl phosphate substrate was added to the cell lysate and incubated at 37 °C for 30 min, after which the reaction was stopped by the addition of NaOH (1 N). The optical density was measured at 405 nm with a microplate reader (calibrated with a standard curve obtained from known concentrations of *p*-nitrophenol) to quantify the amount of *p*-nitrophenol produced. The protein concentration was determined using the micro-BCA protein assay kit from Pierce Chemical (Rockford, IL) with bovine serum albumin as a standard. The ALP activity was determined as the rate of *p*-nitrophenol liberation from *p*-nitrophenyl phosphate, normalized with respect to the total protein content obtained from the same cell lysate and expressed as millimoles of *p*-nitrophenol formation per minute per milligram of total proteins. The amount of calcium deposited by the cells after 14 days of culture in an osteogenic medium was also measured. Briefly, the substrates were washed twice with PBS and soaked in 1 mL of 1 M HCl overnight with shaking to dissolve the calcium mineral. The supernatants were then collected and tested for calcium content by ICP-MS.

For the adipogenic differentiation assay, the cells were cultured in an adipogenic medium containing DMEM supplemented with 10% FBS, 0.5 mM isobutyl-1-methylxanthine, 1 μM dexamethasone, 10 μg/mL insulin, 50 μM indomethacin, 100 U/mL penicillin, 100 μg/mL streptomycin, and 1 μg/mL Fungizone for 14 days. Medium changes were carried out twice weekly. Subsequently, the cells were washed with PBS, fixed with 4% formaldehyde in PBS for 10 min, and stained with Oil Red O for fat globules.

MRI Experiments. MRI experiments were performed at 25 °C in a clinical magnetic resonance (MR) scanner (Siemens

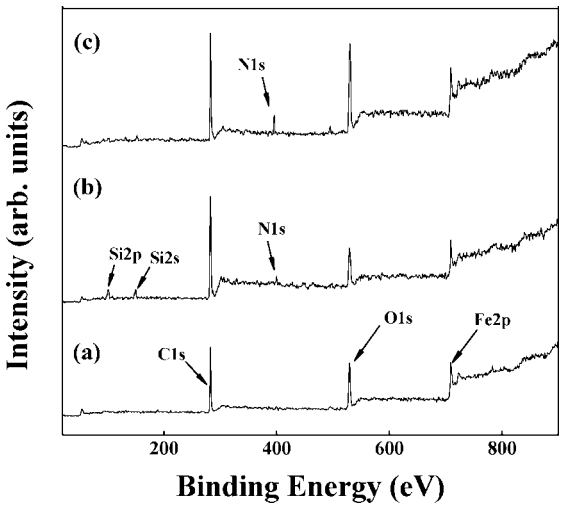

FIGURE 2. XPS wide-scan spectra of SPIONs (a), APTMS-modified SPIONs (b) and CMCS-SPIONs (c).

Symphony; 1.5 T). To demonstrate the T_1 and T_2 effects of the CMCS-SPIONs, these nanoparticles were suspended in tubes of water (20 mL) with iron concentrations at 0.0375, 0.075, 0.15, 0.3, and 0.6 mM Fe. The tubes were placed into the MR scanner, and a number of MR sequences were run: spin echo for R_2 (32 echoes; repetition time (TR) = 1600 ms; echo time (TE) = 15−480 ms) and R_1 (7 TRs; TR = 100−6400 ms; TE = 15 ms) determination. Spin-echo R_1 and R_2 sequences ($n = 8$) were also obtained over a period of 8 and 12 h, respectively, while the samples remained in the scanner to assess the stability of the nanoparticle in solution. The relaxation rates for each sample were computed using the in-house software (MATLAB V7) by fitting of the appropriate exponential functions.

For the MRI experiments with CMCS-SPION-labeled hMSCs, these cells were cultured and labeled as described above. The cells were then washed, counted, and resuspended at a cell density of 500, 1000, 2500, and 5000 cells/mL. The cells were transferred to small plastic tubes in a final volume of 200 μL per tube. The tubes were embedded in 1% agarose and imaged with a clinical 1.5 T magnetic resonance system (Signa, General Electric). Two-dimensional MRI using a gradient echo pulse sequence was performed with the following imaging parameters: TE = 40 ms, TR = 400 ms, slice thickness = 1.5 mm, field of view = 5 × 5 cm, image matrix = 256 × 256.

Statistical Analysis. In each cellular experimental run, at least three samples per time point for each experimental condition were used. The results are reported as mean ± standard deviation and were assessed statistically using one-way analysis of the variance (ANOVA) post-hoc Tukey test. Statistical significance was accepted at $P < 0.05$.

RESULTS AND DISCUSSION

Characterization of CMCS-SPIONs. The success of the covalent attachment of CMCS on SPIONs can be ascertained by comparing the XPS spectra after various stages of surface modification. Parts a−c of Figure 2 show the XPS wide-scan spectra of SPIONs, APTMS-modified SPIONs, and CMCS-SPIONs, respectively. In the wide-scan spectrum of SPIONs (Figure 2a), the predominant components are C 1s (285 eV), O 1s (530 eV), and Fe 2p (710 eV). Carbon is typically present from unavoidable hydrocarbon contamination. The N 1s peak component is not discernible in this spectrum. For APTMS-modified SPIONs, the appearance of the N 1s signal at a binding energy of 400 eV, the Si 2p signal at 100 eV, and the Si 2s signal at 150 eV is consistent with the presence of APTMS on the surface of SPION (Figure 2b). In the case of CMCS-SPIONs (Figure 2c), the increase in the N 1s and O 1s signals that arise from CMCS indicates that CMCS has been successfully immobilized onto the SPIONs.

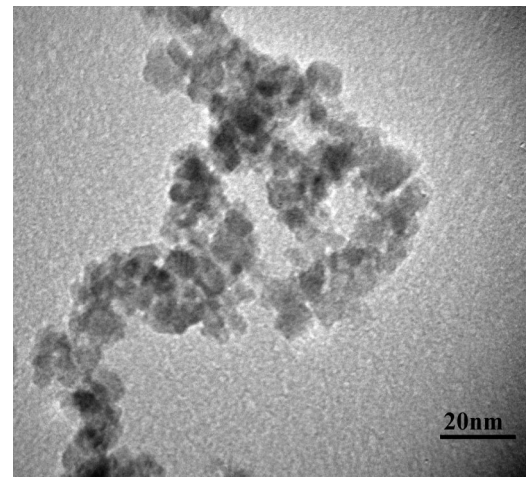

FIGURE 3. TEM image of CMCS-SPIONs.

Table 1. Properties of SPION and CMCS-SPION

	M_s/ emu/g	ζ potential/ mV	hydrodynamic size/ nm	polydispersity
SPION	47.2	−13.6 ± 0.7	32.6 ± 5.5	0.32
CMCS-SPION	41.6	−21.4 ±0.4	55.4 ± 7.1	0.21

TGA was also performed to confirm the presence of the CMCS coating. It is estimated from the TGA results that APTMS and CMCS account for about 4% and 11 % of the weight of CMCS-SPIONs, respectively. In contrast, if the unmodified SPIONs (i.e., without silanization) were coated with CMCS according to the method described by Zhu et al. (36), the CMCS constituted only <4% of the nanoparticles. Thus, the use of APTMS-modified SPIONs with EDC/sulfo-NHS facilitates the formation of a thicker CMCS coating. The ζ potentials of SPIONs and CMCS-SPIONs are −13.6 and −21.4 mV (Table 1). The more negative surface charge of CMCS-SPIONs compared to SPIONs results from −COOH of the carboxymethyl group in CMCS. The saturation magnetization (M_s) values of SPIONs and CMCS-SPIONs are 47.2 and 41.6 emu/g (Table 1), which are deemed sufficient for bioapplications where the M_s values range between 7 and 22 emu/g (37, 38). The decrease in the M_s value can be explained by the presence of the nonmagnetic CMCS coating (29). The size of the individual CMCS-SPIONs is ≤10 nm from the TEM images (Figure 3), while the hydrodynamic sizes of the SPIONs and CMCS-SPIONs are 32.6 and 55.4 nm, respectively (Table 1). The larger hydrodynamic size may be due to some degree of aggregation of the nanoparticles as well as the contribution from the polymeric shell, which does not show up on the TEM images.

Iron Uptake by hMSCs. Surface modification of the nanoparticles is a general strategy to enhance the cellular uptake of nanoparticles. In this report, the surface of SPIONs was modified with CMCS in order to promote the cellular

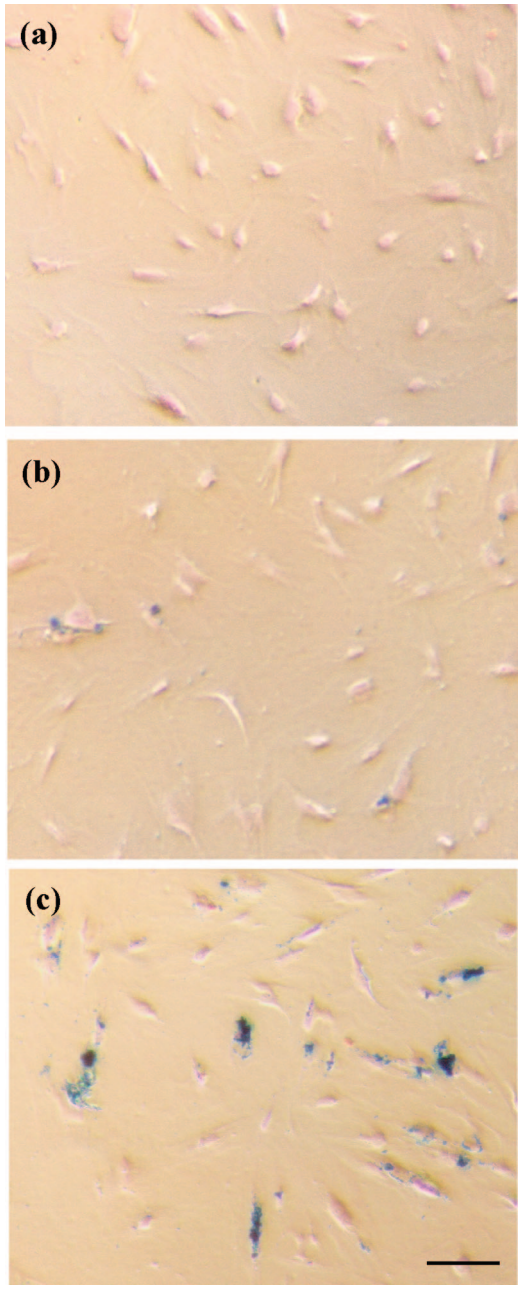

FIGURE 4. Representative Prussian Blue and Nucleus Fast Red counterstained hMSCs incubated without SPIONs (a), with SPIONs (b), and with CMCS-SPIONs (c) for 24 h. 0.05 mg/mL SPIONs or CMCS-SPIONs were used. Scale bar: 100 μm.

uptake. Nanoparticle uptake by hMSCs was visualized using optical microscopy after the cells were grown in a medium with or without nanoparticles for 24 h. The cells were stained with Prussian Blue for the specific detection of intracellular iron. From Figure 4, the presence of many blue particles in cells can be observed when labeling was carried out with CMCS-SPIONs, less so with SPIONs, and no blue particle was seen in the unlabeled cells. TEM examination was used to confirm that the CMCS-SPIONs were internalized by the cells rather than just bonding to the cell membrane. Figure 5a reveals the presence of CMCS-SPIONs, which appeared as black dots in the cytoplasm. Such particles could not be observed in the unlabeled cells (Figure 5b). This intracellular labeling is desired because nanoparticles on the cell membrane may detach and be transferred to other cells in vivo. Furthermore, there is a possibility that membrane-bound particles may interfere with cell−tissue interactions (membrane recognition processes) (20).

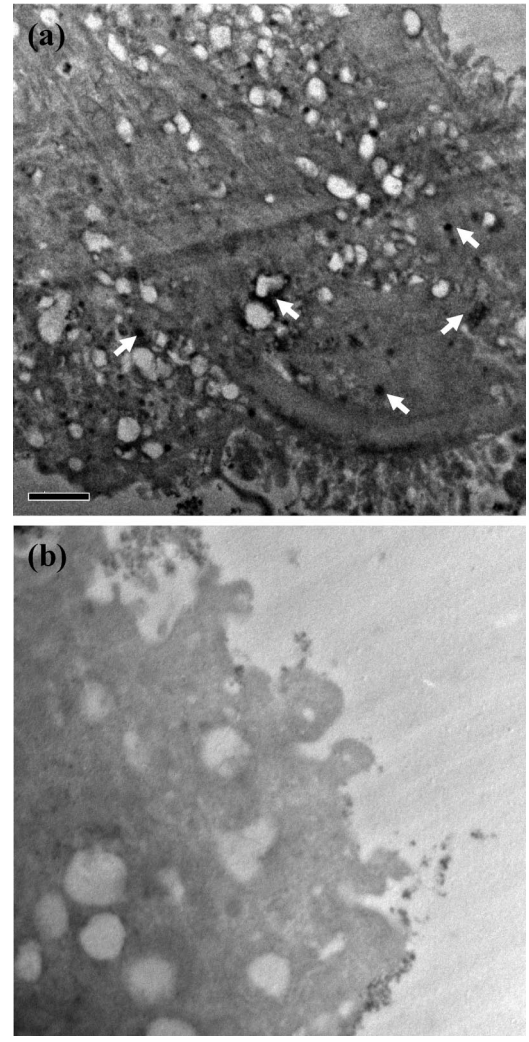

FIGURE 5. TEM image of (a) a cell labeled with CMCS-SPIONs for 24 h (0.05 mg/mL CMCS-SPIONs were used) and (b) an unlabeled cell. White arrows indicate some of the internalized CMCS-SPIONs. Scale bar: 2 μm.

The observation that the amount of CMCS-SPIONs internalized in the hMSCs is much more than that of SPIONs is supported by the quantification of iron uptake by ICP-MS, as shown in Figure 6. CMCS-SPIONs were rapidly internalized into the cells within the first 2 h, and the iron uptake continued to increase with time, reaching 15.6 and 26.7 pg/cell by 6 and 24 h, respectively. In contrast, unlabeled cells exhibited an iron content of ~0.14 pg/cell from the natural intracellular iron source. Thus, for the preparation of the labeled cells for in vitro MR imaging, a labeling time of 24 h was used, and this is consistent with the time used in most of the earlier works on stem-cell labeling by SPIONs (20, 21, 23, 26). The iron content of 26.7 pg/cell after 24 h of labeling with CMCS-SPIONs compares favorably with the results obtained using commercial Feridex with different TAs (10−25 pg/cell) and Resovist with PLL (less than 20 pg/cell) (8, 39).

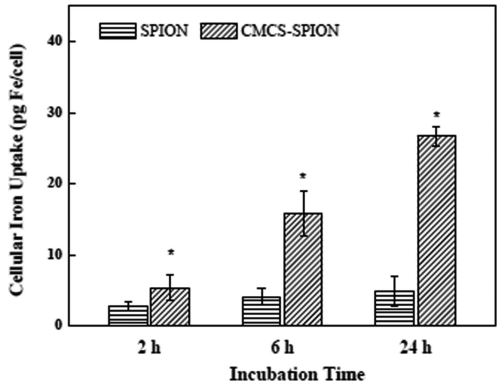

FIGURE 6. Cellular uptake of the different SPIONs (0.05 mg/mL in a medium) after incubation for 2, 6, and 24 h.

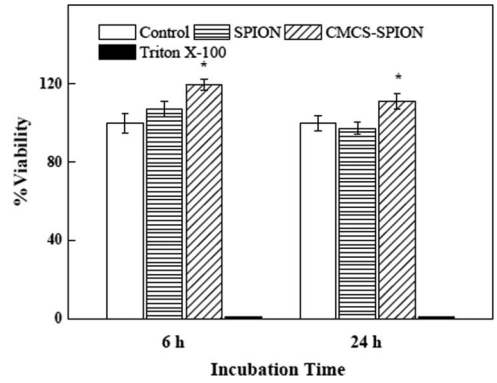

FIGURE 7. Viability of hMSCs grown in media containing 0.05 mg/mL of SPIONs and CMCS-SPIONs. Media without nanoparticles and with 1% Triton X-100 served as the nontoxic and toxic controls, respectively. Asterisks denote significant differences from the control ($P < 0.05$).

The surface properties of iron oxide play a key role in determining its permeability through the cell membrane. Negative surface charges are expected to hamper the phagocytotic uptake as a result of the electrostatic repulsion between the negatively charged particles and negatively charged cell membrane. However, as shown by the results above, the cellular uptake of the CMCS-SPIONs is higher compared to the unmodified SPIONs, even though the former is more negatively charged. Wilhelm et al. have suggested that the high cellular uptake efficiency of anionic nanoparticles may be related, first, to the nonspecific process of nanoparticle adsorption on the cell membrane and, second, to the formation of nanoparticle clusters on the cell surface (40, 41). The authors have shown that bare anionic maghemite nanoparticles exhibit a surprisingly high level of cell internalization, which is comparable with nanoparticles modified with Tat peptide or encapsulated into dendrimers. Similarly, it has been reported that SPIONs with a carboxydextran shell resulted in higher cell uptake compared to SPIONs with a dextran shell (39). Furthermore, it has been shown that CMCS enhances interactions with the cell membrane, possibly because of the interactions of the amine and carboxyl groups of CMCS with the choline moiety (27).

We also investigated whether receptor-mediated endocytosis, which allows rapid accumulation of the nanoparticles compared to the slower nonspecific binding/penetration process, could be another possible mechanism of uptake of CMCS-SPIONs. The presence of receptor-mediated endocytosis was examined by a comparison of the uptake of the CMCS-SPIONs by cells with and without pretreatment with 1 mg/mL of free CMCS for 2 h before incubation in the nanoparticle-containing medium. The results showed no significant decrease in the uptake of CMCS-SPIONs and, hence, the uptake of these nanoparticles is not receptor-mediated.

Cytotoxicity and Cell Differentiation. In the context of efficient cell labeling, the effect of high intracellular iron content on the metabolism of the cells has to be considered. Emerit reported that an intracellular iron overload may lead to cytotoxicity and cell death due to free-radical formation and oxidative stress (42). The viability of hMSCs after labeling with nanoparticles was assessed relative to cells in the control experiment (no nanoparticles present) using the MTT assay, which has been described as a very suitable method for the detection of biomaterial toxicity (34). It can be seen from Figure 7 that hMSCs after labeling with CMCS-SPIONs exhibit 10−20% higher viability compared to the nontoxic control. For SPIONs, no cytotoxicity can be observed as well.

hMSCs have been defined based on their ability to differentiate into several different mesenchymal lineages. Therefore, a possible adverse effect of the labeling procedure on their function has to be investigated. To determine whether the differentiation potential of hMSCs was maintained following labeling, we performed osteogenic and adipogenic differentiation assays for the hMSCs. The results showed that the osteogenic potential was identical with those of control unlabeled hMSCs, as assessed by the alkaline phosphatase activity assay (Figure 8a) and measurement of the calcium deposition (Figure 8b). Oil Red O staining at day 21 following adipogenic differentiation also showed similar neutral lipid vacuoles in both SPION- and CMCS-SPION-labeled cells as the unlabeled cells (Figure 9 and insets).

MRI. Figure 10 shows the inverse relaxation times ($1/T_1$ and $1/T_2$) as a function of the iron molar concentration [Fe]. The R_1 and R_2 values per millimole of iron were found to be 3.86 and 160.5 mM^{-1} s^{-1}, respectively. It is well-known that the relaxivity ratio of R_2/R_1 is an important parameter to estimate the efficiency of T_2 contrast agents. In this work, R_2/R_1 was calculated to be about 40, which is larger than those of the commercial Feridex and Resovist which are in the range of 7 to 17 (43, 44). The stability of CMCS-SPIONs under the 1.5 T magnetic field was also studied by a comparison of the relaxation rates after various periods in the magnetic field. From Figure 10, it can be seen that the results obtained with the CMCS-SPIONs kept in the 1.5 T magnetic field for different periods are not significantly different. The R_1 value obtained at 485 min was 3.83 mM^{-1} s^{-1}, compared to the initial value of 3.86 mM^{-1} s^{-1}. The R_2 value at 720 min was also nearly the same as the initial R_2.

Figure 11 shows the MR images of various concentrations of CMCS-SPION-labeled hMSCs suspended in a low-melting agarose. Compared with control preparations of the agarose medium with unlabeled cells (Figure 11a), the images of the

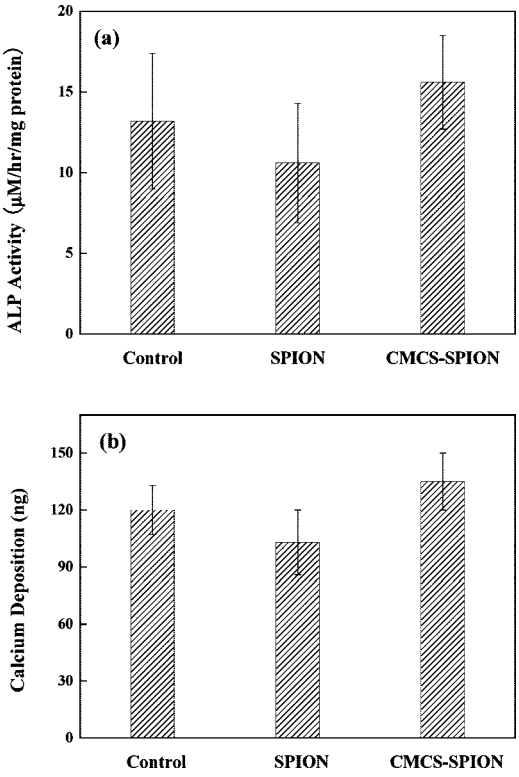

FIGURE 8. (a) ALP activity and (b) calcium mineral deposition of hMSCs cultured without and with the different SPION-containing media (0.05 mg/mL) for 24 h and then further cultured in an osteogenic medium for 14 days.

labeled cells displayed tiny distinct punctuate signal extinctions that clearly contrast against the high signal image background caused by the aqueous agarose medium. The increase in the density of the black dots observed in the MR images of the CMCS-SPION-labeled cells is clearly dependent on the amount of cells used, while the image background of control preparations had a uniform appearance not influenced by the number of cells present. In parts c–e of Figure 11, some spots are observed to be darker and larger than others, owing to both partial volume effects inherent in the imaging parameters and different amounts of the iron label incorporated into each cell. Other possibilities are that there is some overlap between labeled cells and some labeled cells did not provide sufficient contrast for detection. When parts b–e of Figure 11 are compared with Figure 11a, it can be concluded that the tube containing CMCS-SPION-labeled cells at a density of 1000 cells/mL (Figure 11c) can be distinctly differentiated from the control tube (Figure 11a). Because each image slice was 1.5 mm in thickness, it is estimated that the slice shown in Figure 10c contained approximately 40 cells. Lu et al. reported an MRI detection threshold of 6000 cells after uptake of magnetic silica nanoparticles (14). Compared with this value, our results suggest that CMCS-SPIONs as contrast agent have a higher labeling efficiency, which allowed the detection of very low numbers of labeled cells.

CONCLUSION

The surface of SPIONs was conjugated to CMCS, a biopolymer, through a silane linker. The enhanced intracellular uptake of as-prepared CMCS-SPIONs by hMSCs compared to SPIONs was confirmed by optical and electron microscopy and quantitative measurement. It was ascertained that there was no adverse effect on the cell viability and the osteogenic and adipogenic differentiation potentials of hMSCs after labeling with CMCS-SPIONs. The preferential uptake of such nanoparticles by stem cells is likely a result of nonspecific adsorption. As a result of the high labeling efficiency of CMCS-SPIONs, less than 100 labeled cells can be clearly detected by MRI. The reactive group (–COOH) present on the CMCS-SPIONs provides the opportunity for further functionalization of the surface. It is expected that a variety of other biomolecules may be immobilized onto the CMCS-SPIONs to enhance specific cell recognition for use in targeting studies. Thus, CMCS-SPIONs are a promising tool for the labeling of cells for diagnostic and therapeutic applications.

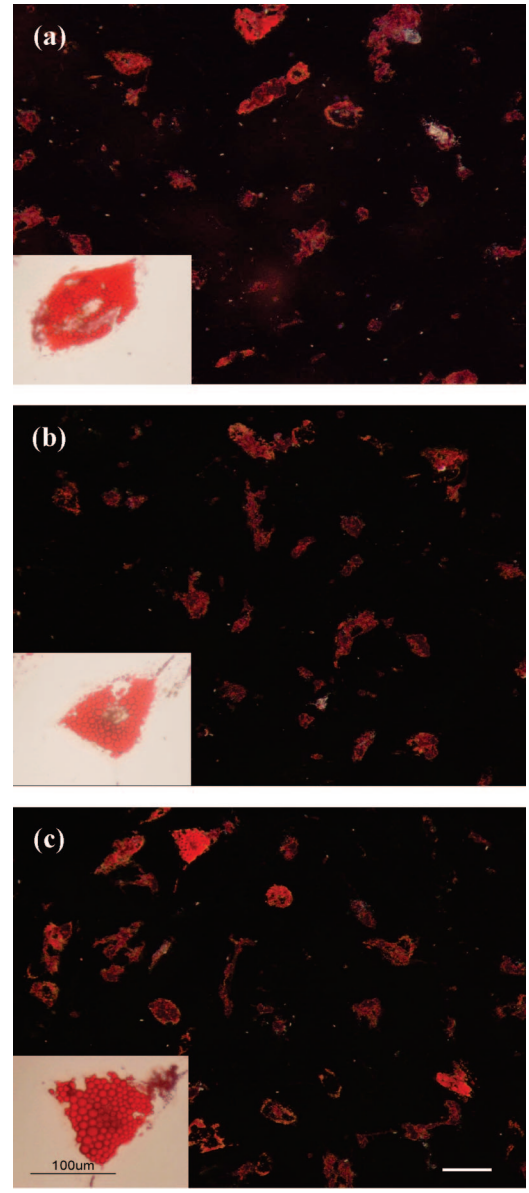

FIGURE 9. Microscopy images of hMSCs cultured without SPIONs (a), with SPIONs (b), and with CMCS-SPIONs (c) containing media (0.05 mg/mL) for 24 h and then further cultured in an adipogenic medium for 14 days. Cells were stained with Oil Red O. Scale bar: 100 μm.

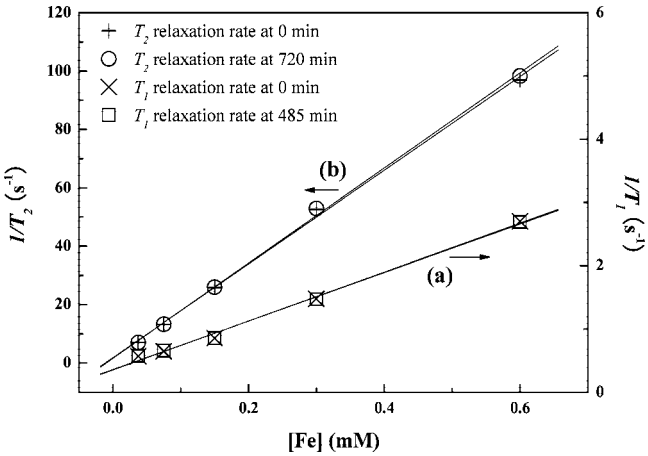

FIGURE 10. Relaxation rates (a) $1/T_1$ (s^{-1}) and (b) $1/T_2$ (s^{-1}) as a function of the iron concentration of CMCS-SPIONs obtained after different time periods under the 1.5 T magnetic field.

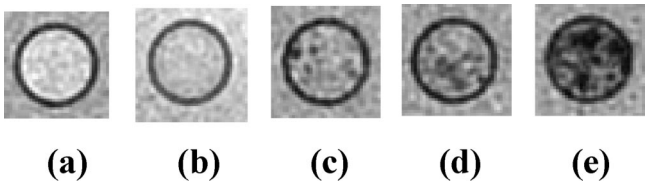

FIGURE 11. MR images of phantoms containing hMSCs (5000 cells/mL) without the nanoparticles (a) and with CMCS-SPION-labeled hMSCs at a cell density of 500 (b), 1000 (c), 2500 (d), and 5000 cells/mL. The cells were suspended in 1% low-melting agarose.

REFERENCES AND NOTES

(1) Pittenger, M. F.; Mackay, A. M.; Beck, S. C.; Jaiswal, R. K.; Douglas, R.; Mosca, J. D.; Moorman, M. A.; Simonetti, D. W.; Craig, S.; Marshak, D. R. *Science* **1999**, *284*, 143–147.

(2) Caplan, A. I. *J. Orthop. Res.* **1991**, *9*, 641–650.

(3) Brazelton, T. R.; Rossi, F. M.; Keshet, G. I.; Blau, H. M. *Science* **2000**, *290*, 1775–1779.

(4) Laurent, S.; Forge, D.; Port, M.; Roch, A.; Robic, C.; Vander Elst, L.; Muller, R. N. *Chem. Rev.* **2008**, *108*, 2064–2110.

(5) Thorek, D. L.; Chen, A. K.; Czupryna, J.; Tsourkas, A. *Ann. Biomed. Eng.* **2006**, *34*, 23–38.

(6) Kraitchman, D. L.; Gilson, W. D.; Lorenz, C. H. *J. Magn. Reson. Imaging* **2008**, *27*, 299–310.

(7) Corot, C.; Robert, P.; Idee, J. M.; Port, M. *Adv. Drug Delivery Rev.* **2006**, *58*, 1471–1504.

(8) Arbab, A. S.; Yocum, G. T.; Kalish, H.; Jordan, E. K.; Anderson, S. A.; Khakoo, A. Y.; Read, E. J.; Frank, J. A. *Blood* **2004**, *104*, 1217–1223.

(9) Bulte, J. W. M.; Kraitchman, D. L. *NMR Biomed.* **2004**, *17*, 484–499.

(10) Terrovitis, J. V.; Bulte, J. W.; Sarvananthan, S.; Crowe, L. A.; Sarathchandra, P.; Batten, P.; Sachlos, E.; Chester, A. H.; Czernuszka, J. T.; Firmin, D. N.; Taylor, P. M.; Yacoub, M. H. *Tissue Eng.* **2006**, *12*, 2765–2775.

(11) Song, H. T.; Choi, J. S.; Huh, Y. M.; Kim, S.; Jun, Y. W.; Suh, J. S.; Cheon, J. *J. Am. Chem. Soc.* **2005**, *127*, 9992–9993.

(12) Heymer, A.; Haddad, D.; Weber, M.; Gbureck, U.; Jakob, P. M.; Eulert, J.; Noth, U. *Biomaterials* **2008**, *29*, 1473–1483.

(13) Ju, S.; Teng, G.; Zhang, Y.; Ma, M.; Chen, F.; Ni, Y. *Magn. Reson. Imaging* **2006**, *24*, 611–617.

(14) Lu, C. W.; Hung, Y.; Hsiao, J. K.; Yao, M.; Chung, T. H.; Lin, Y. S.; Wu, S. H.; Hsu, S. C.; Liu, H. M.; Mou, C. Y.; Yang, C. S.; Huang, D. M.; Chen, Y. C. *Nano Lett.* **2007**, *7*, 149–154.

(15) Gupta, A. K.; Gupta, M. *Biomaterials* **2005**, *26*, 3995–4021.

(16) Wang, Y. X. J.; Hussain, S. M.; Krestin, G. P. *Eur. Radiol.* **2001**, *11*, 2319–2331.

(17) Kustermann, E.; Himmelreich, U.; Kandal, K.; Geelen, T.; Ketkar, A.; Wiedermann, D.; Strecker, C.; Esser, J.; Arnhold, S.; Hoehn, M. *Contrast Media Mol. Imaging* **2008**, *3*, 27–37.

(18) Lewin, M.; Carlesso, N.; Tung, C. H.; Tang, X. W.; Cory, D.; Scadden, D. T.; Weissleder, R. *Nat. Biotechnol.* **2000**, *18*, 410–414.

(19) Josephson, L.; Tung, C. H.; Moore, A.; Weissleder, R. *Bioconjugate Chem.* **1999**, *10*, 186–191.

(20) Bulte, J. W. M.; Douglas, T.; Witwer, B.; Zhang, S. C.; Strable, E.; Lewis, B. K.; Zywicke, H.; Miller, B.; van Gelderen, P.; Moskowitz, B. M.; Duncan, I. D.; Frank, J. A. *Nat. Biotechnol.* **2001**, *19*, 1141–1147.

(21) Babic, M.; Horak, D.; Trchova, M.; Jendelova, P.; Glogarova, K.; Lesny, P.; Herynek, V.; Hajek, M.; Sykova, E. *Bioconjugate Chem.* **2008**, *19*, 740–750.

(22) Frank, J. A.; Miller, B. R.; Arbab, A. S.; Zywicke, H. A.; Jordan, E. K.; Lewis, B. K.; Bryant, L. H., Jr.; Bulte, J. W. *Radiology* **2003**, *228*, 480–487.

(23) Park, B. H.; Jung, J. C.; Lee, G. H.; Kim, T. J.; Lee, Y. J.; Kim, J. Y.; Kim, Y. W.; Jeong, J. H.; Chang, Y. M. *Colloids Surf. A* **2008**, *313*, 145–149.

(24) Arbab, A. S.; Yocum, G. T.; Wilson, L. B.; Parwana, A.; Jordan, E. K.; Kalish, H.; Frank, J. A. *Mol. Imaging* **2004**, *3*, 24–32.

(25) Kumar, M. N.; Muzzarelli, R. A.; Muzzarelli, C.; Sashiwa, H.; Domb, A. J. *Chem. Rev.* **2004**, *104*, 6017–6084.

(26) Horak, D.; Babic, M.; Jendelova, P.; Herynek, V.; Trchova, M.; Pientka, Z.; Pollert, E.; Hajek, M.; Sykova, E. *Bioconjugate Chem.* **2007**, *18*, 635–644.

(27) Zhu, A. P.; Fang, N.; Chan-Park, M. B.; Chan, V. *Biomaterials* **2005**, *26*, 6873–6879.

(28) Zhang, H.; Oh, M.; Allen, C.; Kumacheva, E. *Biomacromolecules* **2004**, *5*, 2461–2468.

(29) Mikhaylova, M.; Kim, D. K.; Berry, C. C.; Zagorodni, A.; Toprak, M.; Curtis, A. S. G.; Muhammed, M. *Chem. Mater.* **2004**, *16*, 2344–2354.

(30) Zhang, C.; Jugold, M.; Woenne, E. C.; Lammers, T.; Morgenstern, B.; Mueller, M. M.; Zentgraf, H.; Bock, M.; Eisenhut, M.; Semmler, W.; Kiessling, F. *Cancer Res.* **2007**, *67*, 1555–1562.

(31) Chen, X. G.; Park, H. J. *Carbohydr. Polym.* **2003**, *53*, 355–359.

(32) Chang, Y. C.; Chen, D. H. *J. Colloid Interface Sci.* **2005**, *283*, 446–451.

(33) Shi, Z.; Neoh, K. G.; Kang, E. T. *Biomaterials* **2005**, *26*, 501–508.

(34) Mosmann, T. *J. Immunol. Methods* **1983**, *65*, 55–63.

(35) Faghihi, S.; Azari, F.; Li, H.; Bateni, M. R.; Szpunar, J. A.; Vali, H.; Tabrizian, M. *Biomaterials* **2006**, *27*, 3532–3539.

(36) Zhu, A.; Yuan, L.; Liao, T. *Int. J. Pharm.* **2008**, *350*, 361–368.

(37) Tartaj, P.; Serna, C. J. *J. Am. Chem. Soc.* **2003**, *125*, 15754–15755.

(38) Xu, C.; Xu, K.; Gu, H.; Zheng, R.; Liu, H.; Zhang, X.; Guo, Z.; Xu, B. *J. Am. Chem. Soc.* **2004**, *126*, 9938–9939.

(39) Mailander, V.; Lorenz, M. R.; Holzapfel, V.; Musyanovych, A.; Fuchs, K.; Wiesneth, M.; Walther, P.; Landfester, K.; Schrezenmeier, H. *Mol. Imaging Biol.* **2008**, *10*, 138–146.

(40) Wilhelm, C.; Gazeau, F. *Biomaterials* **2008**, *29*, 3161–3174.

(41) Wilhelm, C.; Billotey, C.; Roger, J.; Pons, J. N.; Bacri, J. C.; Gazeau, F. *Biomaterials* **2003**, *24*, 1001–1011.

(42) Emerit, J.; Beaumont, C.; Trivin, F. *Biomed. Pharmacother.* **2001**, *55*, 333–339.

(43) Rohrer, M.; Bauer, H.; Mintorovitch, J.; Requardt, M.; Weinmann, H. J. *Invest. Radiol.* **2005**, *40*, 715–724.

(44) Qin, J.; Laurent, S.; Jo, Y. S.; Roch, A.; Mikhaylova, M.; Bhujwalla, Z. M.; Muller, R. N.; Muhammed, M. *Adv. Mater.* **2007**, *19*, 2411–2411.

AM8000538